

# Investigation of the effect of discrete absorbers upon the measurement of blood volume with near-infrared spectroscopy

Michael Firbank, Eiji Okada and David T Delpy

Department of Medical Physics and Bioengineering, University College London, 11–20 Capper Street, London WC1E 6JA, UK

Received 20 September 1996

**Abstract.** This paper derives an analytical model for investigating the effect of the distribution of absorbers upon light attenuation in a scattering medium. Results from this are found to agree with those of Monte Carlo simulations. The implications of this model are then examined for their likely effect upon the measurement of cerebral blood volume (CBV) using near-infrared (NIR) spectroscopy. We conclude that, given the small diameter of the majority of cerebral blood vessels, the distribution of the blood will have little effect upon the measurement of CBV. Where changes to the blood volume occur in the larger ( $> 0.2$  mm diameter) vessels on the surface of the brain, NIR spectroscopy is likely to underestimate the change.

## 1. Introduction

Near-infrared (NIR) spectroscopy is used to monitor changes in blood oxygenation by measuring changes in the attenuation of NIR light passing through tissue (Wyatt *et al* 1990, Edwards *et al* 1988, Hampson and Piantadosi 1988, De Blasi *et al* 1993, Elwell *et al* 1994). Light is both scattered and absorbed by tissue, and the absorption is usually assumed to occur uniformly throughout the tissue. However, blood, the principal absorber in tissue, is confined to veins, arteries and capillaries, and it is the purpose of this study to investigate what (if any) effect this partitioning has. Of particular interest is the relationship between changes in the absorption of the blood and the resultant change in light attenuation.

Liu *et al* (1995) examined the likely consequences of the absorbing blood being confined to vessels using an experimental model consisting of a polyester-based light-scattering cylinder (Firbank and Delpy 1993, Kurth *et al* 1995) with absorbing and scattering liquid (intralipid) flowing through internal channels. From measurements of the change in light attenuation with absorption, they derived an empirical formula for the equivalent absorption coefficient, i.e. the absorption coefficient possessed by an equivalent homogeneous medium which has the same overall attenuation properties.

We present here a more analytical approach to the problem, which we believe sheds some light on the physics of the situation, and is more appropriate at small detector/source separations. This analysis is compared with Monte Carlo simulations, and with the theory of Liu *et al* (1995).

## 2. Theory

For a homogeneous medium, the light distribution resulting from an incident beam of collimated light can be calculated from diffusion theory (Patterson *et al* 1989, Arridge *et al* 1992). We want to adapt the diffusion theory so that it can deal with an array of absorbing centres in an otherwise homogeneous medium.

In this paper our medium is a slab of finite thickness, but infinite height and breadth, which scatters light with a transport scattering coefficient of  $\mu'_s$  and an absorption coefficient of  $\mu_a$ . A solution of the diffusion equation for this geometry is provided in Kohl *et al* (1995), which provides the number of photons leaving per unit area,  $\Gamma(x, L)$  as a function of source–detector separation  $x$  and the photon pathlength,  $L$ .

We wish to introduce to this homogeneous slab some absorbing vessels (see figure 1) with absorption coefficient  $\mu_a^v$ . The vessels have a radius  $r$ , and are infinitely long. Looking at a 2D slice, the vessels occupy a relative fractional cross-sectional area of  $f_v$  and the area of the surrounding medium is hence  $A(1 - f_v)$ .

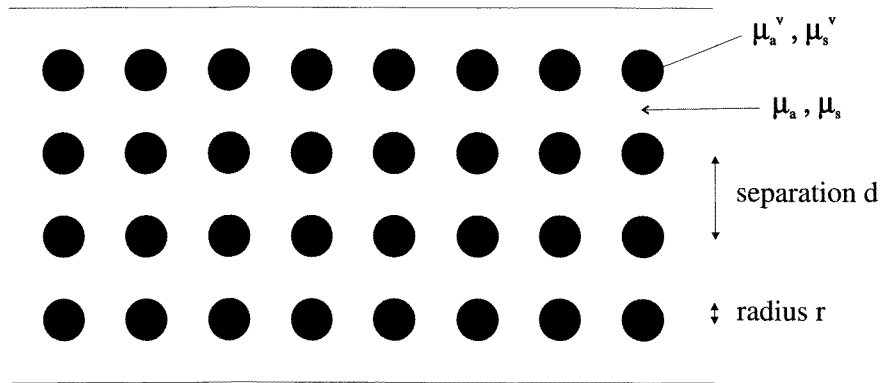


**Figure 1.** The arrangement of the absorbers and slab used in the simulations.

In a simple view of the situation, we can imagine that the vessels do not disturb the distribution of the paths taken by the light, but only affect the intensity. Photons which exit having travelled a distance  $L$  will have randomly encountered vessels, with the probability of intersecting  $n$  holes being  $P(n, L)$ . At any particular exit position,  $x$ , the attenuation of the emerging light will be determined by the distribution of photon pathlengths  $\Gamma(x, L)$  and by the distribution of the number of vessels encountered. We assume that the average photon path through a vessel is equal to its diameter, and that the attenuation will be given by this pathlength and the absorption  $\mu_a^v$  of the vessel. By multiplying the probability of a photon having a given pathlength with the probability of it encountering  $n$  vessels, and integrating over all possible pathlengths and number of holes, we obtain the total number of photons exiting per unit area, the exitance  $\Gamma(x)$ :

$$\Gamma(x) = \int_{L=0}^{\infty} \Gamma(x, L) \sum_{n=0}^{\infty} P(n, L) \exp(-\mu_a^v n 2r) dL. \quad (1)$$

In practice, we calculated the integral over all photon pathlengths using a discrete sum. The upper bound and  $dL$  were calculated from the mean pathlength (in the absence of vessels), which can be simply calculated from the diffusion theory. The upper bound for

the integration was set at three times the mean pathlength, and  $dL$  equal to this value divided by 400.

Since the vessels are all internal to the diffusing region, the light must travel a certain distance before encountering a vessel. We define  $L'$  as that part of a photon's pathlength during which it can encounter vessels. After initially entering the scattering medium, the distance a photon must traverse before hitting a vessel is approximately equal to the vessel separation,  $d$ . As the photons are subject to random scattering, the total distance actually travelled will be  $\simeq \mu_s d^2$ , thus

$$L' = L - d^2 \mu_s. \quad (2)$$

The probable distribution of the photon having struck  $n$  holes is given by the Poisson distribution:

$$P(n) = \frac{\exp(-L'/\lambda)}{n!} \left(\frac{L'}{\lambda}\right)^n. \quad (3)$$

The collision length,  $\lambda$ , is the mean length travelled by a photon between interactions with the vessels, and can be defined

$$\lambda = \frac{k}{N2r\epsilon} \quad (4)$$

$N$  being the number of vessels per unit area,  $k$  a constant dependent upon the geometry of the situation and  $\epsilon$  the fraction of colliding photons which are not reflected from the vessel surface (see section 2.4). After substituting for  $N$ , this equation can be rewritten

$$\lambda = \frac{k\pi r(1 - f_v)}{2f_v\epsilon}. \quad (5)$$

From a comparison of this theory and the Monte Carlo results, we used  $k = 1.236$

We henceforth refer to equation (1) as the random-hole model in order to distinguish it from the diffusion equation.

### 2.1. Liu's equation

We compare results in this paper with the empirical formula given by Liu *et al* (1995) for an effective absorption coefficient  $\overline{\mu}_a$  which can be used in a homogeneous diffusion equation. This is reproduced here for reference:

$$\overline{\mu}_a = \mu_a + \beta f_v (\mu_a^v - \mu_a) \exp[-r(\mu_a^v - \mu_a)] \quad (6)$$

$\beta$  being a constant which depends upon the optical properties of the medium. In their experiments on a phantom, they found  $\beta$  to be equal to 0.74, and hypothesized that it might vary with the refractive index difference between the vessels and the surrounding medium, and with the scattering anisotropy factor,  $g$ .

### 2.2. Monte Carlo modelling

The Monte Carlo model used was based on a previously published model (Hiraoka *et al* 1993) which had been altered to include vessels with different absorption and scattering coefficients in a regular rectangular array (see figure 1). A slab geometry was used, with a thickness of 40 mm. The scattering coefficient  $\mu_s$  was  $1.0 \text{ mm}^{-1}$ , with  $\mu_s$  of the vessels  $= 0.01 \text{ mm}^{-1}$ . The absorption coefficient of the scattering medium  $\mu_a$  was  $0.007 \text{ mm}^{-1}$ . The anisotropy factor  $g$  was 0, i.e. isotropic scattering was assumed in all cases except for one investigation (see section 3.2) having  $g = 0.9$ . In this latter case,  $\mu'_s = (1 - g)\mu_s$  was

kept equal to  $1.0 \text{ mm}^{-1}$ . The model was run for a variety of different radii, absorption coefficients and distances between vessels. A typical run of the model followed 50 million photons.

### 2.3. Partial pathlength

It has been shown (Hiraoka *et al* 1993) that the mean path length  $\bar{L}$  taken by light exiting from a scattering medium at point  $x$  is:

$$\bar{L} = -\frac{1}{\Gamma(x)} \frac{d\Gamma(x)}{d\mu_a}. \quad (7)$$

The partial path through a particular region of this scattering medium is similarly found  $\bar{L}_v = (1/\Gamma)(d\Gamma/d\mu_a^v)$ , with  $d\mu_a^v$  being the change in absorption coefficient through the region. We define the fractional partial path as the ratio of the partial to total pathlength:

$$\ell_v = \frac{\bar{L}_v}{\bar{L}}. \quad (8)$$

This gives a direct measure of how much a change in the optical properties of a region affects the measured attenuation, i.e. the contribution of that region to the signal.

If the vessels had the same optical properties as the surrounding tissue, and were uniformly distributed through the tissue, the fractional partial path in the vessels would be identical with the ratio of vessel volume to total tissue volume. On the other hand, if the vessels were extremely absorbing and sparsely dispersed, their fractional partial path would be almost zero, since light which passes through the vessels would be absorbed and only light which had avoided the vessels would be detected.

The measurement of absolute blood volume using NIR spectroscopy as described by Wyatt *et al* (1990) essentially uses these equations to find the relative path length in the blood vessels. In this case, the absorption coefficient is altered by changing the oxygenation of the blood.

### 2.4. Effect of refractive index

If the refractive index of the vessel is different to that of the surrounding medium, there will be a reflection at the boundary, and not all of the light which is incident on the vessel will penetrate into it. The fraction of light reflected will depend on the angular distribution of light incident on the vessel.

If the vessels are in a medium with a scattering length comparable to (or shorter than) the mean spacing between the vessels, it is likely that the light will be incident upon a vessel at random angles.

The distribution of incident angles,  $I(\theta)$ , with respect to the normal to the vessel's surface will hence be

$$I(\theta) = \cos(\theta) \sin(\theta). \quad (9)$$

The percentage of reflected light for a given incident angle will be given by the Fresnel equation

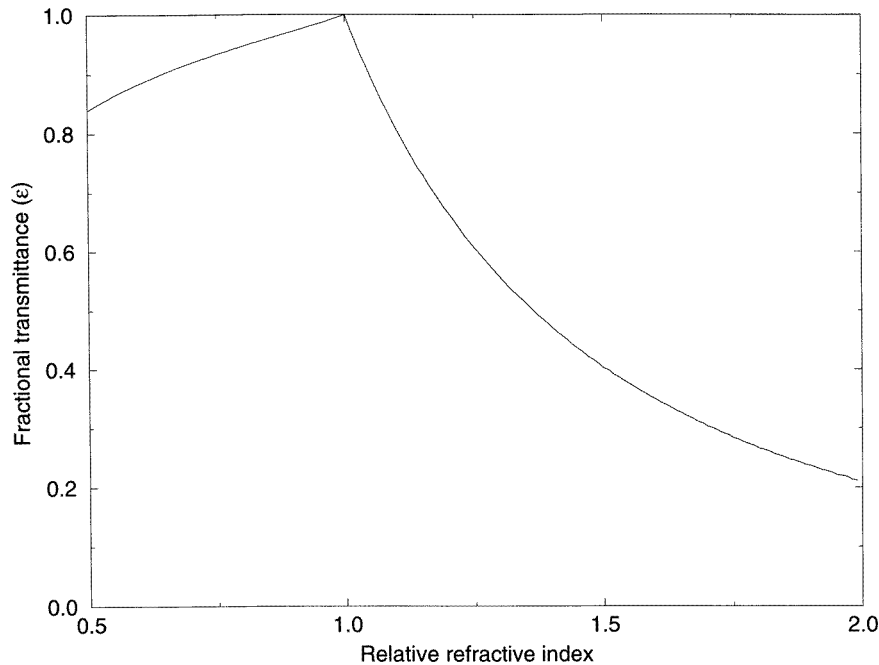
$$R(\theta) = \left( \frac{\cos(\theta) - n_{12} \cos(\theta')}{\cos(\theta) + n_{12} \cos(\theta')} \right)^2 + \left( \frac{n_{12} \cos(\theta) - \cos(\theta')}{n_{12} \cos(\theta) + \cos(\theta')} \right)^2 \quad (10)$$

where  $n_{12}$  is the relative refractive index and  $\theta'$  is the refracted angle. For angles greater than the critical angle  $\theta_c = \sin^{-1}(1/n_{12})$ , all light is reflected and  $R = 1$ . Using these equations we can find the average reflection  $\bar{R}$  :

$$\bar{R} = \int_0^{\pi/2} \frac{\cos(\theta) \sin(\theta) R(\theta) d\theta}{\cos(\theta) \sin(\theta) d\theta}. \quad (11)$$

$\epsilon$  is the fraction of the light which has penetrated into the vessel, and hence

$$\epsilon = 1 - \bar{R}. \quad (12)$$



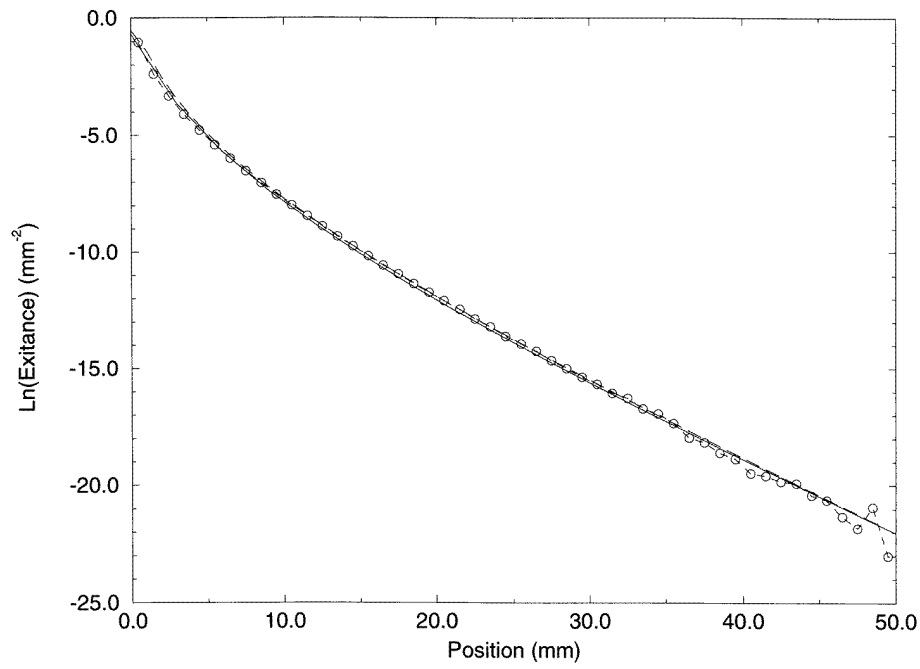
**Figure 2.** The fraction of incident light which is transmitted into the vessels as a function of the relative refractive index.

Figure 2 shows a graph of  $\epsilon$  versus the relative refractive index.

### 3. Results

#### 3.1. Comparison of models

Figure 3 shows the exitance  $\Gamma$  as a function of detector position (for a source at  $x = 0$ ) as calculated by the Monte Carlo model, the random-hole model and diffusion theory for a vessel separation of 1.86 mm and radii 0.25 mm. Figure 4 shows a calculation of the total pathlength and the vessel pathlength for the same geometry and models. There is almost no discernible difference between the random-hole and diffusion models in these graphs, and both agree well with the Monte Carlo data. In figure 5 are shown the fractional partial paths  $\ell_v$  through the vessels for a variety of vessel spacings and radii (all vessels having an absorption coefficient of  $0.4 \text{ mm}^{-1}$ ). These figures show that at large ( $> 30 \text{ mm}$ ) detector positions all three models agree, but at closer detector positions, the random-hole



**Figure 3.** Exitance versus source/detector spacing for:  $\circ$ - - - $\circ$ , Monte Carlo; —, random-hole model; - - -, homogeneous diffusion theory.

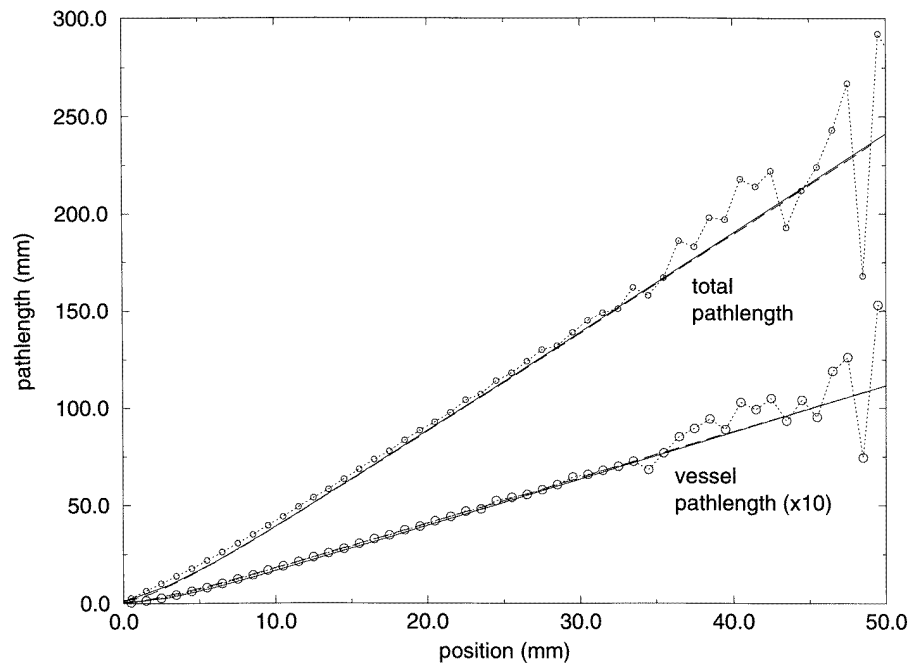


**Figure 4.** Partial and total pathlength as a function of source/detector spacing:  $\circ$ - - - $\circ$ , Monte Carlo model; —, random-hole model; - - -, homogeneous diffusion theory.

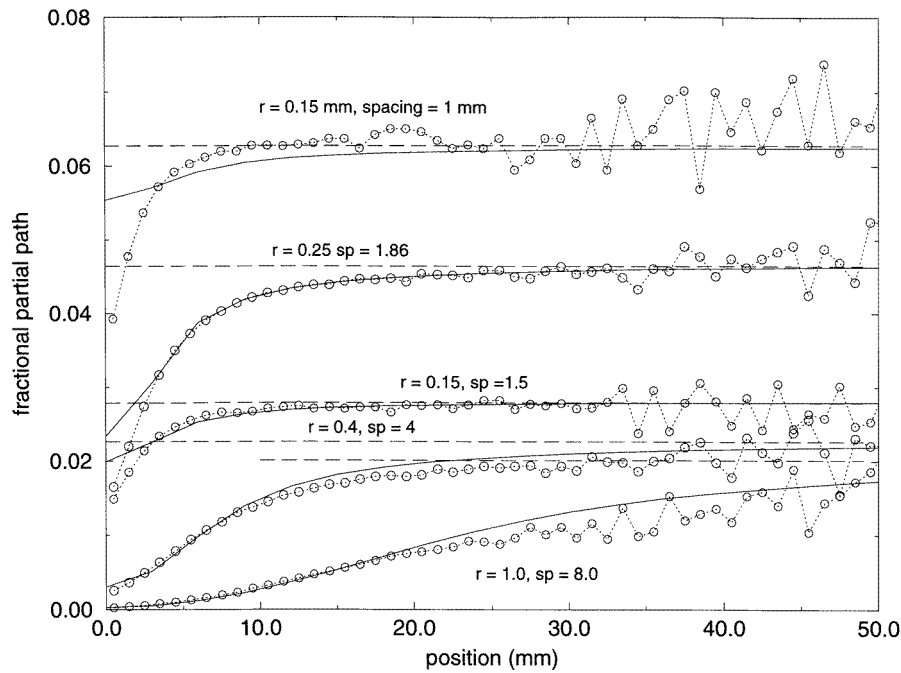


**Figure 5.** Fractional partial pathlengths for assorted vessel diameters and spacings for the three different models: —, random-hole; - - -, homogeneous diffusion theory; ○- - -○, Monte Carlo.

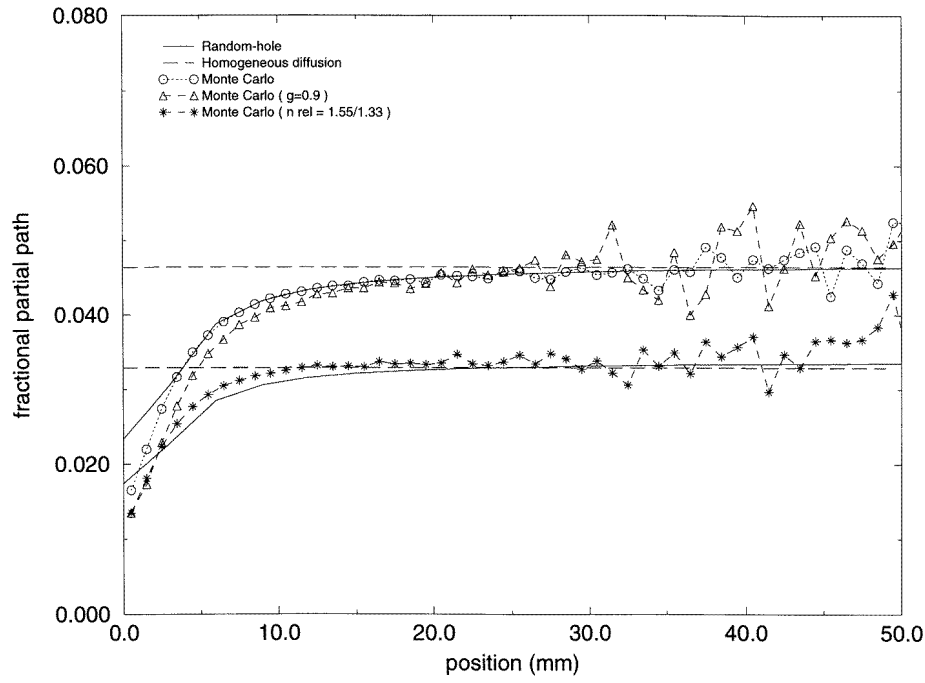
model (equation (1)) provides a much better agreement with the results of Monte Carlo modelling than using a homogeneous diffusion theory with Liu *et al*'s 'effective absorption coefficient'. This is because this latter model does not take into account the relatively low probability of encountering a vessel for photons with short paths.

### 3.2. Effect of refractive index and $g$

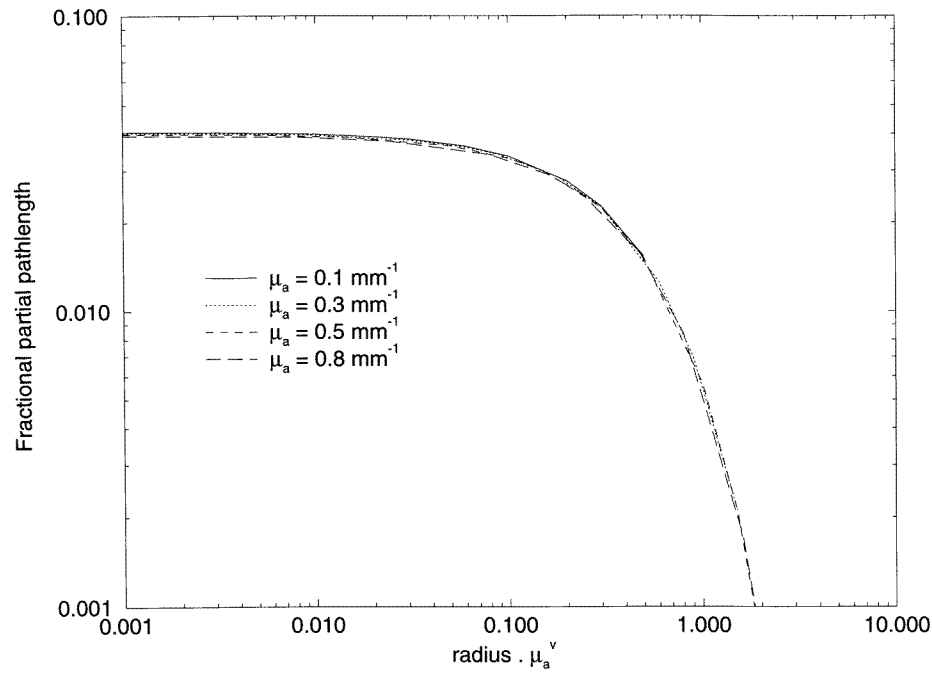
Figure 6 shows a comparison of the partial path length through the vessels for matched refractive indices and  $n_{12} = 1.55/1.33$ . For the latter case,  $\epsilon$  is calculated as 0.7088 from equation (12). This value has also been used for  $\beta$  in equation (6).

Figure 6 also shows the effect on the partial path of changing the anisotropy factor,  $g$ , of the scattering medium from 0 to 0.9. The transport scattering coefficient  $\mu'_s = \mu_s(1 - g)$  is kept at  $1.0 \text{ mm}^{-1}$  in both cases. This figure shows that, as expected, the anisotropy factor has little effect upon  $\ell_v$ , except close to the source. In studies on phantoms, however, the refractive index mismatch has a significant effect, and obviously has to be borne in mind.

For a resin/intralipid based phantom,  $n_{12} \simeq 1.55/1.35 = 1.165$  and  $\epsilon$  can be calculated as 0.73, which agrees well with the empirical value of  $\beta = 0.74 \pm 0.02$  published in Liu *et al* (1995). Since the anisotropy factor has negligible effect at large source/detector spacings, we can conclude that the  $\beta$  factor in equation (6) depends only upon refractive index.  $\beta$  appears to be identical with  $\epsilon$ , and can thus be calculated from equation (12).



**Figure 6.** Showing the effect of refractive index and anisotropy factor,  $g$ , on the fractional partial pathlength for a radius of 0.25 mm and vessel spacing of 1.86 mm.



**Figure 7.** The fractional partial pathlength of the vessels versus the product of  $\mu_a^v$  and radius.

### 3.3. Effect of radius/ $\mu_a$

Figure 7 shows, for a large source/detector spacing, the partial pathlength in the vessels against the product of  $\mu_a^v$  and  $r$ , for a number of different values of  $\mu_a^v$  ranging from  $0.1 \text{ mm}^{-1}$  to  $0.8 \text{ mm}^{-1}$ . This shows that with  $\mu_a^v r$  less than 0.03, the fractional partial path is almost constant, but at bigger values of  $\mu_a^v r$ ,  $\ell_v$  falls.

When measuring attenuation spectra in tissue, of course, the vessel radius is generally a constant, whereas the absorption will vary with wavelength. Figure 8 shows the absorption coefficients of water and haemoglobin (2.0 mMol, average saturation 70%). If we assume a homogeneous distribution of the blood in the tissue, using a typical blood volume of 4%, the average absorption coefficient  $\bar{\mu}_a = \mu_a(1 - f_v) + f_v\mu_a^v$ . This can be used in the diffusion equation,  $f_v$  being 0.04 with  $\mu_s = 1 \text{ mm}^{-1}$ . Figure 9 shows the resulting attenuation spectrum at 40 mm spacing, and figure 10 the differences between this spectrum and spectra calculated with the haemoglobin confined to vessels of differing radii. The differences become larger as the radius increases.

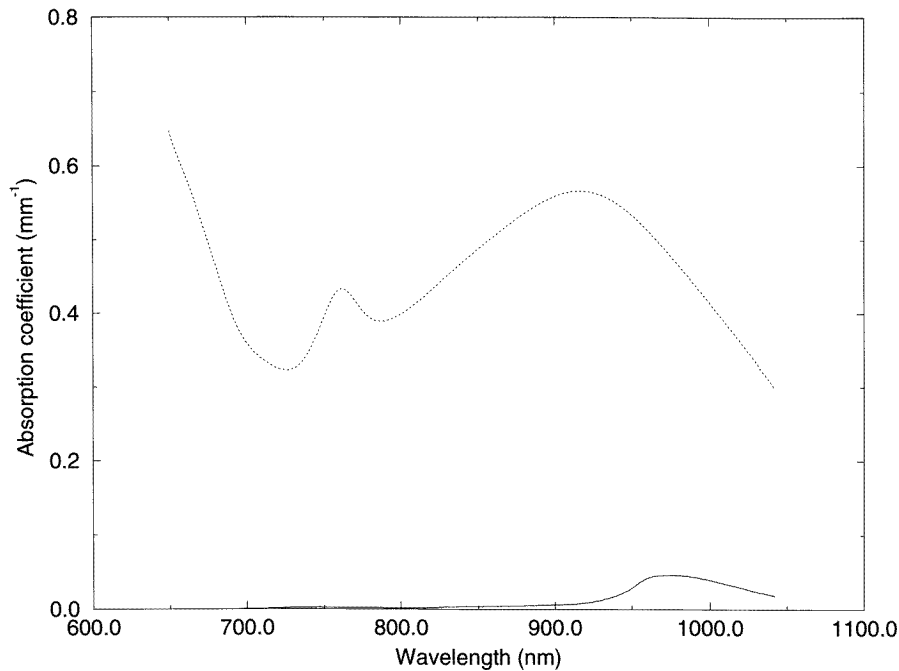


**Figure 8.** The absorption coefficient of: ·····, haemoglobin (2.0 mMol, 70% saturation); —, water.

### 3.4. Effect of scattering coefficient

Figure 11 shows the fractional pathlength  $\ell_v$  for vessels with a radius of 0.25 and spacing of 1.86 mm when  $\mu_s^v = 0.01 \text{ mm}^{-1}$ ,  $\mu_s^v = \mu_s = 1.0 \text{ mm}^{-1}$  and with  $\mu_s^v = 4.0 \text{ mm}^{-1}$ .  $\ell_v$  drops a little as  $\mu_s$  varies, but not by a great deal. Changing the vessel scattering coefficient from 0.01 to  $1.0 \text{ mm}^{-1}$  reduces  $\ell_v$  by approximately 1% and even increasing  $\mu_s^v$  to  $4.0 \text{ mm}^{-1}$  only decreases  $\ell_v$  by 5%. This effect is probably dependent upon the vessel size, and becomes less significant as the diameter drops.

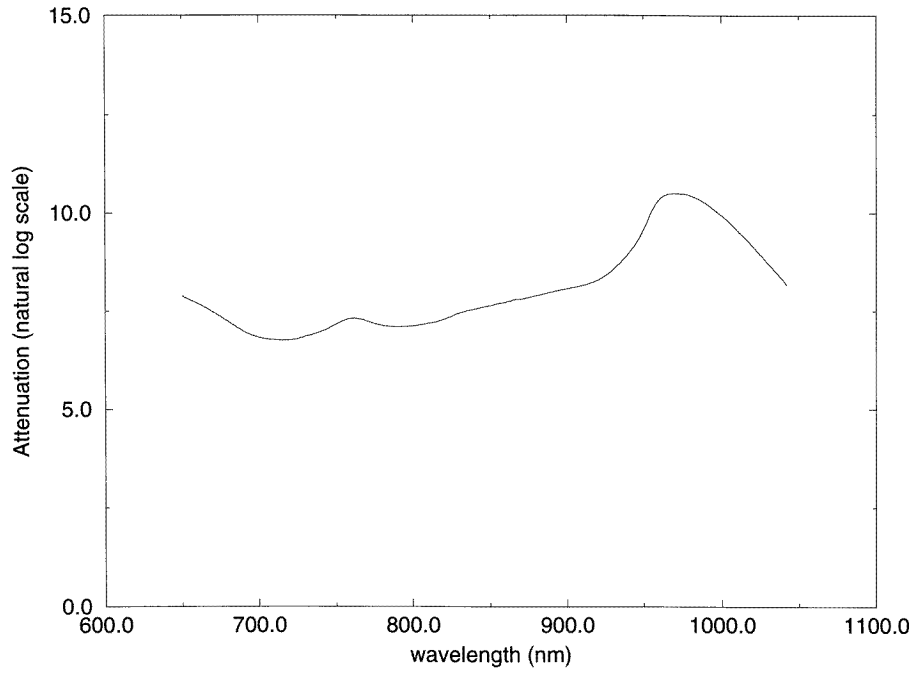


**Figure 9.** The attenuation spectra at a source/detector spacing of 40 mm for a homogeneous medium with an absorption equivalent to vessels ( $\mu_a^v = 0.4 \text{ mm}^{-1}$ ) occupying a fraction = 0.04 of the cross-sectional area.

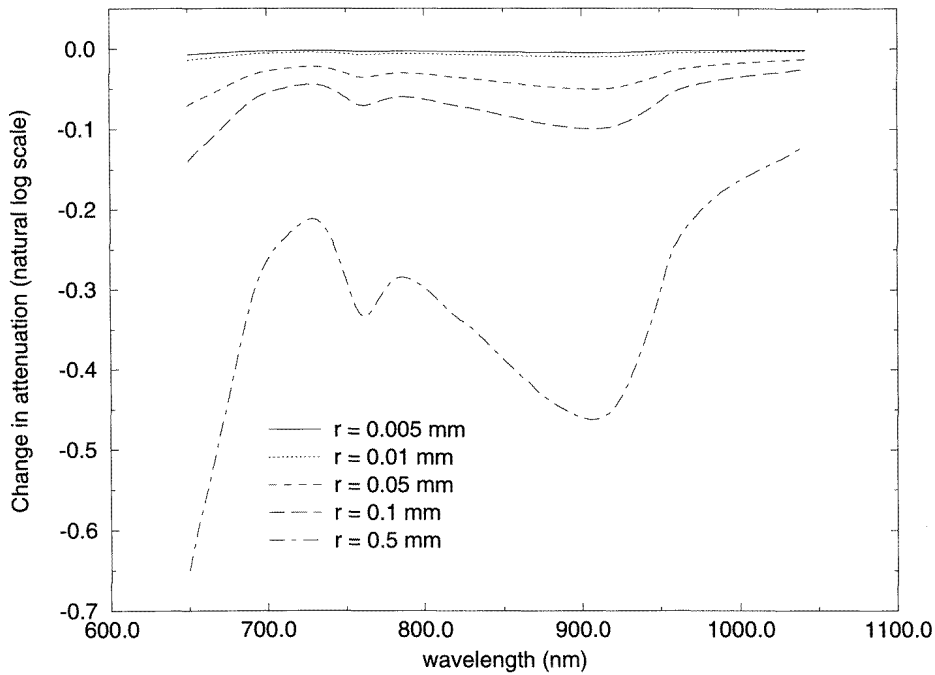


**Figure 10.** Deviations in the attenuation from the homogeneous absorption case to vessels of different radii.

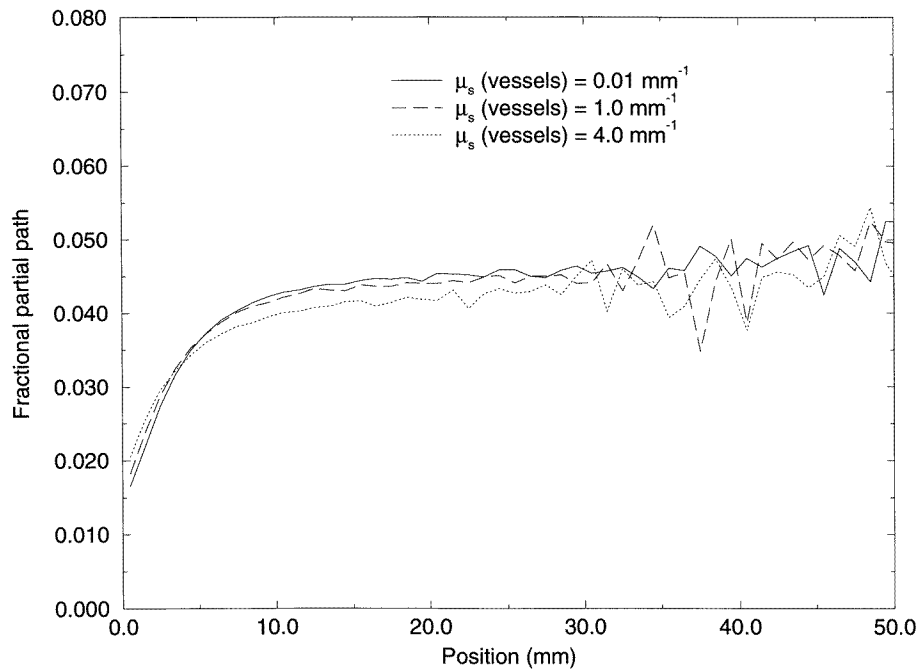


Figure 11. Fraction partial pathlength  $\ell_v$  for vessels with differing scattering properties.

#### 4. Discussion

Figure 7 shows that the effect of the absorption coefficient depends upon the size of the vessels. For values of  $\mu_a^v r < 0.03$  the attenuation is equivalent to that in a homogeneous medium with the absorption uniformly distributed. At higher values of  $\mu_a^v r$ , the light effectively ‘sees’ less of the vessels, since light which penetrates them is attenuated a great deal, and hence is not detected. This has an effect on both a measurement of the apparent vessel volume, and on the attenuation spectrum, which is shown in figure 8.

The anisotropy factor,  $g$ , seems to have no effect on the measurement at large detector spacings, and only a small effect at small spacings. This is probably because the light undergoes sufficient scattering events to become randomized in its directionality. It is probable, however, that as the fractional volume occupied by the vessels increases,  $g$  will have an increased effect as the light will have less scattering medium within which to scatter and become diffuse. The volume of blood in the brain is approximately 4% (Sakai *et al* 1985), equivalent to the volumes studied here, and it is therefore unlikely that the  $g$  value will have any effect in tissue. Changes in the scattering coefficient of the blood are also unlikely to have any effect upon a measurement of blood volume.

In resin/water models, the relative refractive indices make a difference to the penetration of light into the vessels, but in tissue it is unlikely to have a great deal of effect, since tissue and blood have similar refractive indices, close to 1.4 (Bolin *et al* 1989). Differences in refractive index may have some influence for blood vessels in adipose tissue, however, where, due to its high lipid content ( $\simeq 70\%$  in adults), the refractive index is  $\simeq 1.46$ . In this case,  $\epsilon$  is 0.91, and a measurement of the blood volume in adipose tissue would be approximately 10% too low. The refractive index of brain has not been measured,

unfortunately, but since its average lipid content is only about 10% (compared with 4% for muscle), so its refractive index is likely to be close to 1.4.

The concentration of haemoglobin in the blood of the major arteries and veins is approximately  $150 \text{ g l}^{-1}$  (2.3 mM). According to absorption spectra published by Matcher *et al* (1995) and assuming an oxygen saturation of 70% this gives an absorption coefficient of 0.36 (at 700 nm), 0.45 at 800 nm (the isobetic point of Hb, HbO<sub>2</sub>) and 0.65 (at 950 nm). In the arterioles and capillaries of the brain, the haematocrit is 30% lower than the main arteries (Lammertsma *et al* 1984) and hence the absorption coefficient will be 30% lower.

The main cerebral arteries entering the parenchyma from the base of the brain are approximately 1 mm in diameter. These branch into arteries of 0.2 mm in diameter, and these in turn branch into smaller vessels. Most of the vessels which penetrate into the cortex have a diameter of 0.04 mm (Duvernoy *et al* 1981). Hudetz *et al* (1987) investigating the pial arteries of rats found that the branching ratio of the arteries was 4.14, with the average vessel radius decreasing by 0.63 at each branch. The distance between forks was not found to be related to the diameter of the branch. Since all the vessels internal to the brain, and the vast majority on its surface, are less than 0.2 mm diameter, they will have an approximately equal contribution to the detected signal.

Given the general distribution of cerebral vessel diameters, a measurement of the change in light attenuation on the head resulting from a change in oxygenation will give a good estimate of the blood volume in the *head*, provided that the mean pathlength is known. To determine the blood volume in the brain, of course, we need to know the partial pathlength of light through the brain (Elwell *et al* 1994).

Changes in the large main arteries and veins, however, will have less effect on the detected NIR signal. This implies that changes to the cerebral blood volume which occur principally in the few large external vessels on the cortical surface may be underestimated by NIR spectroscopy.

## Acknowledgments

The authors would like to thank the EPSERC (grant GR/K077386), the Japan Society for the promotion of science and Hamamatsu Photonics for financial support

## References

- Arridge S R, Cope M and Delpy D T 1992 The theoretical basis for the determination of optical pathlengths in tissue: temporal and frequency analysis *Phys. Med. Biol.* **37** 1531–60
- Bolin F P, Preuss L E, Taylor R C and Ference R J 1989 Refractive index of some mammalian tissues using a fiber optic cladding method *Appl. Opt.* **28** 2297–303
- De Blasi R A, Cope M, Elwell C E, Safoue F and Ferrari M 1993 Noninvasive measurement of human forearm oxygen consumption by near-infrared spectroscopy *J. Appl. Physiol.* **67** 20–5
- Duvernoy H M, Delon S and Vannson J L 1981 Cortical blood vessels of the human brain *Brain Res. Bull.* **7** 519–79
- Edwards A D, Wyatt J S, Richardson C E, Delpy D T, Cope M and Reynolds E O R 1988 Cotside measurement of cerebral blood flow in ill newborn infants by near-infrared spectroscopy *The Lancet* **2** 770–1
- Elwell C E, Cope M, Edwards A D, Wyatt J S, Delpy D T and Reynolds E O R 1994 Quantification of adult cerebral haemodynamics by near-infrared spectroscopy *J. Appl. Physiol.* **77** 2753–60
- Firbank M and Delpy D T 1993 A design for a stable and reproducible phantom for use in near infrared imaging and spectroscopy *Phys. Med. Biol.* **38** 847–53
- Hampson N B and Piantadosi C A 1988 Near infra red monitoring of human skeletal muscle oxygenation during forearm ischaemia *J. Appl. Physiol.* **64** 2449–57

- Hiraoka M, Firbank M, Essenpreis M, Cope M, Arridge S R, van der Zee P and Delpy D T 1993 A Monte Carlo investigation of optical pathlength in inhomogeneous tissue and its application to near-infrared spectroscopy *Phys. Med. Biol.* **38** 1859–76
- Hudetz A G, Conger K A, Halsey J H Jr, Pal M, Dohan O and Kovach A G B 1987 Pressure distribution in the pial arterial system of rats based on morphometric data and mathematical models *J. Cereb. Blood Flow Metabol.* **7** 342–55
- Kohl M, Essenpreis M and Cope M 1995 The influence of glucose concentration upon the transport of light in tissue-simulating phantoms *Phys. Med. Biol.* **40** 1267–87
- Kurth C D, Liu H, Thayer W S and Chance B 1995 A dynamic phantom brain model for near-infrared spectroscopy *Phys. Med. Biol.* **40** 2079–92
- Lammertsma A A, Brooks D J, Beaney R P, Turton D R, Kensett M J, Heather J D, Marshall J and Jones T 1984 In vivo measurement of regional cerebral haematocrit using positron emission tomography *J. Cereb. Blood Flow Metabol.* **4** 317–22
- Liu H, Chance B, Hielscher A H, Jacques S L and Tittel F K 1995 Influence of blood vessels on the measurement of hemoglobin oxygenation as determined by time-resolved reflectance spectroscopy *Med. Phys.* **22** 1209–17
- Matcher S J, Elwell C E, Cooper C E, Cope M and Delpy D T 1995 Performance comparison of several published tissue near-infrared spectroscopy algorithms *Anal. Biochem.* **227** 54–68
- Patterson M S, Chance B and Wilson B C 1989 Time resolved reflectance and transmittance for the non invasive measurements of tissue optical properties *Appl. Opt.* **28** 2331–6
- Sakai F, Nakazawa K, Tazaki Y, Ishii K, Hino H, Igarashi H and Kanda T 1985 Regional cerebral blood volume and hematocrit measured in normal human volunteers by single photon emission computed tomography *J. Cereb. Blood Flow Metabol.* **5** 207–13
- White D R, Widdowson E M, Woodard H Q and Dickerson W T 1991 The composition of body tissues (II) Fetus to young adult *Br. J. Radiol.* **64** 149–59
- Wyatt J S, Cope M, Delpy D T, Richardson C E, Edwards A D, Wray S and Reynolds E O R 1990 Quantitation of cerebral blood volume in human infants by near-infrared spectroscopy *J. Appl. Physiol.* **68** 1086–91